Interplay between percolation and glassiness in the random Lorentz gas

Giulio Biroli,[1] Patrick Charbonneau ◉,[2,3] Eric I. Corwin ◉,[4] Yi Hu ◉,[2,*] Harukuni Ikeda ◉,[5] Grzegorz Szamel ◉,[6] and Francesco Zamponi ◉[1]

[1]*Laboratoire de Physique de l'Ecole Normale Supérieure, ENS, Université PSL, CNRS, Sorbonne Université, Université de Paris, F-75005 Paris, France*
[2]*Department of Chemistry, Duke University, Durham, North Carolina 27708, USA*
[3]*Department of Physics, Duke University, Durham, North Carolina 27708, USA*
[4]*Department of Physics and Material Science Institute, University of Oregon, Eugene, Oregon 97403, USA*
[5]*Graduate School of Arts and Sciences, The University of Tokyo, Tokyo 153-8902, Japan*
[6]*Department of Chemistry, Colorado State University, Fort Collins, Colorado 80523, USA*

The random Lorentz gas (RLG) is a minimal model of transport in heterogeneous media that exhibits a *continuous* localization transition controlled by void space percolation. The RLG also provides a toy model of particle caging, which is known to be relevant for describing the *discontinuous* dynamical transition of glasses. In order to clarify the interplay between the seemingly incompatible percolation and caging descriptions of the RLG, we consider its exact mean-field solution in the infinite-dimensional $d \to \infty$ limit and perform numerics in $d = 2 \dots 20$. We find that for sufficiently high d the mean-field caging transition precedes and prevents the percolation transition, which only happens on timescales diverging with d. We further show that activated processes related to rare cage escapes destroy the glass transition in finite dimensions, leading to a rich interplay between glassiness and percolation physics. This advance suggests that the RLG can be used as a toy model to develop a first-principle description of particle hopping in structural glasses.

Introduction. The random version of the venerable Lorentz gas (RLG) consists of a tracer navigating between a collection of Poisson-distributed hard spherical obstacles. Despite the apparent simplicity of the model, its phenomenology is quite rich. As the obstacle density increases, tracer diffusion is first delayed and then suppressed altogether. In physical dimensions, $d = 2, 3$, the localization transition provably coincides with that of void space percolating [1,2], and is hence continuous and accompanied by an extended subdiffusive regime [3–5]. The minimal yet complex nature of the RLG makes it a standard model of transport in heterogeneous media for systems as diverse as electrons in metals with impurities [6] and proteins in cells [7,8].

The RLG also plays a key role in the theory of glasses. Its consideration was an important step toward formulating the mode-coupling theory (MCT) of glasses [9–12], and has provided key insight into the role of pinning particles in deeply supercooled liquids [13–16]. The RLG can further be construed as a limit of a hard-sphere binary mixture [17–19] with one component—the obstacles—being infinitely smaller than the infinitely dilute other—the tracer. (Exchanging obstacle and tracer sizes recovers Fig. 1(a) [12].) If the analogy suggested by this special limit holds, one might then expect the RLG model to be part of the hard-sphere glass universality class. Studying its behavior in high dimension d could there-

fore also shed light on large-d corrections to the mean-field theory of glasses [20].

In this Letter, we resolve the interplay between percolation and glassiness in the RLG. We first formulate a mean-field theory (MFT) of the RLG, which becomes exact in the infinite-dimensional limit $d \to \infty$. We find analytically that in this limit, the RLG undergoes a dynamical arrest of the MCT type, identical to that of hard-sphere glasses in the same limit [20], which confirms the binary mixture analogy. A fundamental inconsistency, however, follows from this result [Fig. 1(a)]: on the one hand, in finite, low d, the exact mapping of the RLG to a percolation transition gives rise to a *continuous* localization transition [3–5,12]; on the other hand, MFT predicts a *discontinuous* caging transition. The simplest possible resolution, namely, that the nature of the percolation transition might change in the $d \to \infty$ limit, was recently ruled out [21]. Hence, some nontrivial corrections to MFT must play an important role for RLG physics.

In order to probe these effects, we investigate the problem numerically in $d = 2 \dots 20$ and obtain accurate percolation thresholds (up to $d = 9$) as well as static and dynamical descriptions of caging. Three main insights follow from this study. (i) MFT provides the exact $d \to \infty$ dynamics over finite timescales, during which the dynamical arrest prevents the tracer from exploring the percolating network of cages. (ii) MFT fails to capture the $d \to \infty$ percolation transition because the long-time and large-dimensional limits do not commute. (MFT holds when one first takes the large-dimensional limit, whereas the percolation transition relies
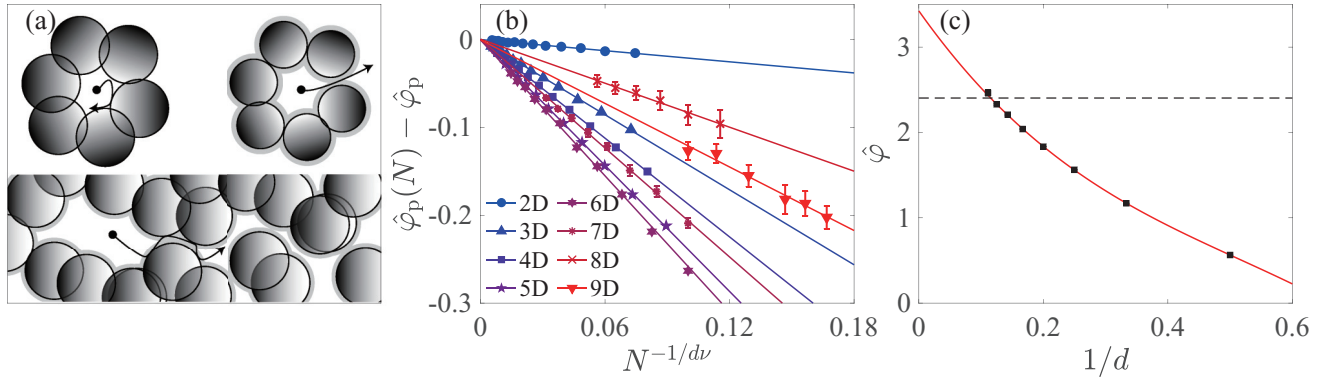
_____
*yi.hu@duke.edu

FIG. 1. (a) Two descriptions of RLG uncaging upon decreasing $\hat{\varphi}$: Top: The MFT cage discontinuously disintegrates at $\hat{\varphi}_d$. Bottom: cages merge continuously and form an infinite percolating cluster at $\hat{\varphi}_p$. (b) Finite-size scaling of $\hat{\varphi}_p(N)$ in $d = 2$ to 9. (c) $\hat{\varphi}_p(\infty)$ in $d = 2$ to 9 (squares, from right to left) compared with the MFT $\hat{\varphi}_d$ (dashed line). The red line denotes a polynomial fit to the percolation thresholds, Eq. (3). Extrapolating this form strongly suggests that $\lim_{d \to \infty} \hat{\varphi}_p > \hat{\varphi}_d$.

on processes taking place on a timescale that diverges with d.) (iii) The percolating network of cages is explored through *activated* hopping events, which happen with probability vanishing exponentially with d, and can be analytically described by instantonic corrections of MFT. These events are expected to play a key role in glass formation and yet have thus far eluded theoretical grasp. We thus conclude that the RLG is a toy model of some of the key activated processes in glasses, and is simple enough to be treated analytically and numerically, thus opening the way for a first-principle description of such processes.

Mean-field theory derivation. The MFT of glass-forming liquids, which becomes exact in the $d \to \infty$ limit [20], predicts the existence of a dynamical (MCT-like) transition, at which the long-time limit of the scaled mean-squared displacement (MSD), $\hat{\Delta} = d\Delta$, jumps from diverging diffusively to a finite value. Because the infinitely asymmetric binary fluid mixture that coincides with the RLG in the $d \to \infty$ limit might, however, be singular, we here sidestep this analogy by directly solving the model by cavity reconstruction. Writing the explicit partition function for the RLG and using the replica symmetric construction of Refs. [20,22,23], one obtains a self-consistent expression for $\hat{\Delta}$:

$$\frac{1}{2\hat{\varphi}} = -\hat{\Delta} \int_{-\infty}^{\infty} dh \, e^h \ln q(\hat{\Delta}/2, h) \frac{\partial q(\hat{\Delta}/2, h)}{\partial \hat{\Delta}}, \quad (1)$$

at the dimensionally rescaled packing fraction $\hat{\varphi} = \rho V_d/d$, where ρ is the number density of obstacles, V_d is the volume of d-dimensional unit sphere [23], and $q(\hat{\Delta}, h) = \{1 + \text{erf}[(h + \hat{\Delta}/2)/\sqrt{2\hat{\Delta}}]\}/2$. Equation (1) gives that a dynamical glass transition takes place at $\hat{\varphi}_d = 2.4034\ldots$, half that for $d \to \infty$ hard spheres [22].

Considering that $\hat{\Delta}$ is an order parameter for both the percolation and the glass transitions, one may expect the theory of glasses to also describe percolation criticality. This is not the case. While the cage size is expected to diverge logarithmically in mean-field percolation [21], the MFT cage size is twice that of hard spheres, i.e., $\hat{\Delta} = 2\hat{\Delta}_{HS}(2\hat{\varphi})$, and thus also presents a square-root singularity upon approaching $\hat{\varphi}_d$, i.e., $\hat{\Delta}(\hat{\varphi}_d) - \hat{\Delta}(\hat{\varphi}) \sim \sqrt{\hat{\varphi} - \hat{\varphi}_d}$. In other words, we here confirm that RLG and hard-sphere fluids share a same MFT univer-

sality class characterized by a discontinuous glass transition, which is distinct from that of simple percolation.

Percolation threshold. Although the percolation criticality is distinct from that of the dynamical glass transition, one might nonetheless wonder whether the former smoothly extrapolates to the latter in the limit $d \to \infty$. We thus consider the scaling of the percolation threshold, $\hat{\varphi}_p$, with dimension to determine if it coincides with the MFT prediction for $\hat{\varphi}_d$ in the $d \to \infty$ limit. In systems with N Poisson-distributed obstacles in a d-dimensional box under periodic boundary conditions, the void percolation can be mapped onto the bond percolation of a network built on the Voronoi tessellation of obstacles [24]. We here assign each edge of that tessellation the smallest obstacle radius σ that can block it, and use a disjoint-set forest algorithm adapted from continuum-space analysis to identify the percolated cluster [25,26]. Optimizing the periodic boundary conditions [23,27] and the Voronoi tessellation [23,28,29] enables us to obtain $\hat{\varphi}_p(N)$ up to $d = 9$. The thermodynamic $\hat{\varphi}_p$ is then extracted by fitting [Fig. 1(b)]

$$|\hat{\varphi}_p(N) - \hat{\varphi}_p| \sim N^{-1/d\nu}, \quad (2)$$

where ν is the percolation correlation length exponent [23,30].

For $d \leqslant 8$, $\hat{\varphi}_p < \hat{\varphi}_d$, but for $d = 9$ $\hat{\varphi}_p = 2.46(4) > \hat{\varphi}_d$, indicating that the order of the two switches between $d = 8$ and 9. Fitting the results to a cubic form,

$$\hat{\varphi}_p = 3.42(8) - 10.3(9)\frac{1}{d} + 13(3)\left(\frac{1}{d}\right)^2 - 9(4)\left(\frac{1}{d}\right)^3, \quad (3)$$

further suggests that $\lim_{d \to \infty} \hat{\varphi}_p = 3.42(8)$, which differs significantly from the MFT prediction [Fig. 1(c)]. In other words, while MFT is expected to be exact in $d \to \infty$ limit, it fails to capture the percolation transition in that same limit. A densifying system in $d > 8$ thus first encounters around $\hat{\varphi}_d$ (imperfect) local cages that percolate on larger scales, and can be escaped via activated hopping processes [31], before being properly localized at the percolation threshold $\hat{\varphi}_p$.

Cage sizes. In order to ascertain this scenario, the MFT description of caging needs first to be assessed. To do so, we implement a cavity reconstruction scheme adapted from Refs. [23,31,32], which can be viewed as the continuum-space generalization of the Leath algorithm [33]. Specifically, we define a hyperspherical shell, centered at the origin, of inner
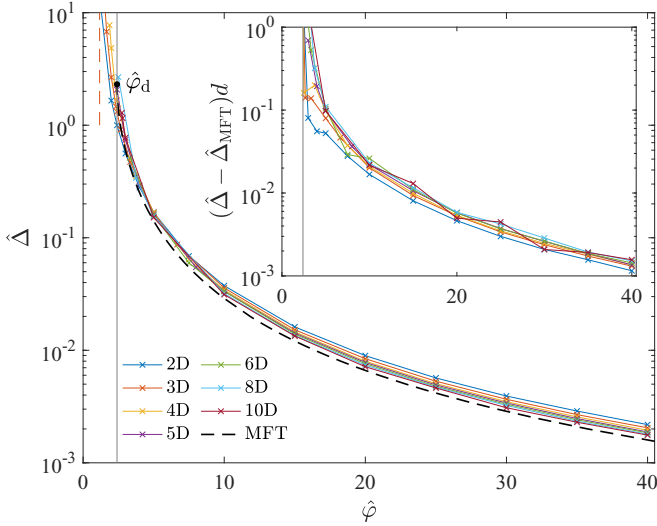
FIG. 2. Scaling of the cage size with density for different d. Results for $d = 2$–6 are obtained by random sampling, and those for $d \geqslant 8$ from the long-time caging dynamics. At high densities, the MFT, $d \to \infty$ prediction (dashed line) is steadily approached as d increases, but at small densities the percolation criticality dominates the growth of the cage size (e.g., in $d = 3$ the cage size diverges upon approaching $\hat{\varphi}_p$ (red dashed line)). Note that results in high dimension and small densities are numerically inaccessible. Inset: The scaling collapse of the deviation from the MFT prediction identifies the dominant $1/d$ correction.
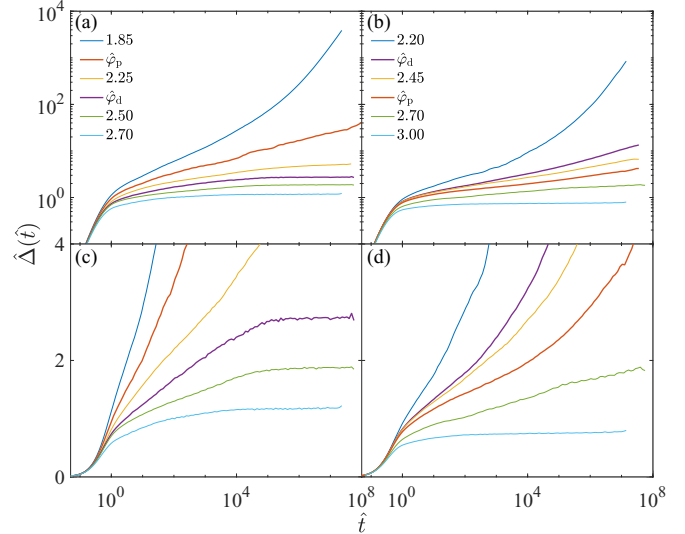

FIG. 3. Time evolution of the MSD in the ballistic dynamics in (a) $d = 6$ and (b) 10 under log-log scale, and (c),(d) for the same dimensions under log-lin scale. The long-time dynamics is diffusive for $\hat{\varphi} < \hat{\varphi}_p$ and localized for $\hat{\varphi} > \hat{\varphi}_p$. In $d \geqslant 6$, $\hat{\Delta}$ at $\hat{\varphi}_p$ is expected to grow logarithmically at long times. In (d), specifically, the signature of an intermediate dynamical slowdown emerges before that logarithmic growth.

radius σ and outer radius $r_{\max}$, and pick a number of obstacles N from the Poisson distribution $p(N) = N_0^N e^{-N_0}/N!$ with $N_0 = d\hat{\varphi}(r_{\max}^d - \sigma^d)$, which are then placed uniformly at random within that shell. (The cutoff $r_{\max}$ must be large enough that the results do not depend on it.) This algorithm guarantees that the probability of obtaining a cavity, $\mathbb{C}$, containing the origin exactly tracks the distribution of cavities at that same $\hat{\varphi}$ in an infinitely large system. A set of randomly distributed points $\{S_i\}$ within $\mathbb{C}$ can then be used to compute the second moment of the coordinates,

$$\Delta(\mathbb{C}) = \langle (S_i - S_j)^2 \rangle = 2(\langle S_i^2 \rangle - \langle S_i \rangle^2), \qquad (4)$$

and then $\Delta = \mathbb{E}_\mathbb{C}[\Delta(\mathbb{C})]$. Physically, this method provides the long-time limit of the MSD of a tracer without explicitly running its dynamics, which is advantageous because it eliminates putative dynamical bottlenecks. However, because its computational cost increases exponentially with d, for $d \geqslant 8$ the explicit long-time limit of the tracer dynamics needs to be computed to estimate Δ. The agreement between the two approaches at intermediate d nevertheless indicates that bottlenecks can be confidently neglected in this regime.

For $\hat{\varphi} \gg \hat{\varphi}_d$, the (scaled) cage size nicely converges to the MFT prediction as d increases (Fig. 2), and the dominant correction is perturbative in $1/d$. In this high-density regime, the quantitative consistency with MFT is robust down to physical dimensions. A generalized MFT with perturbative corrections should thus offer accurate predictions in all d, a clear opportunity for future theoretical studies.

By contrast, for $\hat{\varphi} \sim \hat{\varphi}_d$, a regime dominated by percolation criticality—with Δ diverging at $\hat{\varphi}_p$—is observed (Fig. 2). The

static cage size either crosses $\hat{\varphi}_d$ smoothly or is expected to diverge before reaching $\hat{\varphi}_d$ from above, depending on the relative order of $\hat{\varphi}_d$ and $\hat{\varphi}_p$. These strong discrepancies with respect to MFT found around $\hat{\varphi}_d$ hint at a complex interplay between glass and percolation physics.

Tracer dynamics. In order to disentangle the two phenomena, we consider the dynamical counterpart of the above static description. We first examine the tracer dynamics, following the ballistic approach of Höfling *et al.* [5,34], setting the microscopic timescale such that the short-time growth of the MSD scales as $\hat{\Delta}(t) = \hat{t}^2$ when $\hat{t} \to 0$ in all dimensions. As expected from percolation theory [4,21], in the long-time limit either localization or diffusion is observed, for $\hat{\varphi} > \hat{\varphi}_p$ and $\hat{\varphi} < \hat{\varphi}_p$, respectively [Figs. 3(a) and 3(b)]. An intermediate subdiffusive regime, which scales logarithmically with time for $d \geqslant 6$ [21], also develops around the percolation threshold, and fully dominates the dynamics at $\hat{\varphi} = \hat{\varphi}_p$. Figures 3(c) and 3(d) consider more closely the interplay between $\hat{\varphi}_p$ and $\hat{\varphi}_d$. In $d = 6$, no hint of MFT-like caging is observed around $\hat{\varphi}_p$, as expected. Because $\hat{\varphi}_p < \hat{\varphi}_d$, percolation dominates the caging dynamics. Hence, for $\hat{\varphi} > \hat{\varphi}_p$, logarithmic growth immediately follows the ballistic regime until a plateau is reached. By contrast, in $d = 10$, where $\hat{\varphi}_p > \hat{\varphi}_d$, a weak dynamical slowdown emerges at intermediate times for $\hat{\varphi} \gtrsim \hat{\varphi}_d$. Such a preasymptotic effect is distinctly absent in lattice systems [21]. However, conclusively determining whether this slowdown is controlled by MFT caging or by some other model-specific preasymptotic correction to percolation criticality would require higher-dimensional systems than this computational scheme currently permits.

To pinpoint the origin of this weak dynamical slowdown, we instead seek an observable more sensitive to MFT-like
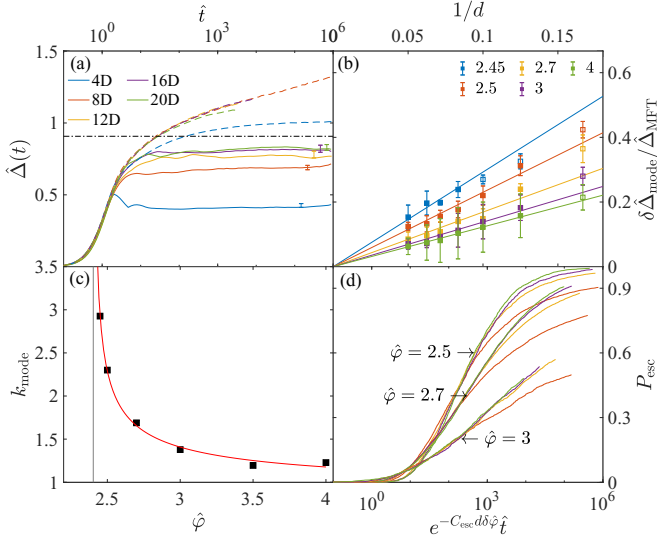
FIG. 4. Cages and cage escapes in $d = 4$–20 obtained from dynamical cavity reconstructions. (a) Modal (solid line) and mean- (dashed line) squared displacements of tracers with time at $\hat{\varphi} = 2.7$, along with the MFT prediction (dash-dotted line). MSD curves terminate when 2% of tracers have escaped. While the MSD drifts with time, the mode robustly plateaus. (b) The plateau of $\hat{\Delta}_{\text{mode}}$ approaches the MFT prediction as in Eq. (5) for various $\hat{\varphi}$. Error bars are obtained from bootstrapping and also reported in panel (a) for reference. (c) The scale of the perturbative correction to the cage size grows upon approaching $\hat{\varphi}_{\text{d}}$, and empirically fits $k_{\text{mode}} = 0.46/\sqrt{\delta\hat{\varphi}} + 0.81$. (d) Cage escape probabilities for $\hat{\Delta}_{\text{esc}} = 4$ in $\hat{\varphi} = 2.5$, 2.7, and 3 collapse under an instantonic form with empirical prefactor $C_{\text{esc}} = 0.4$.

caging. Recalling that percolation criticality is dominated by rare large cages, while MFT is evaluated via a saddle point that extracts the *typical* cage size, we choose to focus on the *modal* cage size, i.e., $\hat{\Delta}_{\text{mode}}(t) = \arg\max P[(\Delta(t)]$ [23]. By construction, $\hat{\Delta}_{\text{mode}}$ eliminates the contribution of rare large cages and cage escapes, and thus effectively plays the same role as the generalized MSD considered in recent glass studies [31,35]. This observable is further amenable to a dynamical version of the static cavity reconstruction. Although this setup misses finite-yet-large cages, it provides a sufficiently broad span of the cage-size distribution to reliably identify $\hat{\Delta}_{\text{mode}}$. It also extends the numerically accessible dimensional range. Results up to $d = 20$ and averaged over at least 2×10^3 independent samples with $\hat{\Delta}_{\text{max}} = d(r_{\text{max}} - \sigma)^2 \geqslant 14$ are reported in Fig. 4. We find that $\hat{\Delta}_{\text{mode}}$ plateaus quickly after the ballistic regime, even near $\hat{\varphi}_{\text{p}}$, and that this plateau steadily approaches the MFT caging prediction as d increases [Fig. 4(a)], even for $\hat{\varphi}_{\text{d}} < \hat{\varphi}_{\text{p}}(d)$ in $d > 8$. Note that a small finite-size correction due to finiteness of the shell thickness appears in the highest dimension considered, $d = 20$, but the convergence to the MFT prediction remains within the statistical error range [23].

Remarkably, the approach to the MFT prediction exhibits a perturbative $1/d$ correction [Fig. 4(b)],

$$\hat{\Delta} = \hat{\Delta}_{\text{MFT}} - \frac{k_{\text{mode}}}{d}, \tag{5}$$

even fairly close to $\hat{\varphi}_{\text{d}}$. Fitting the modal cages with Eq. (5) [Fig. 4(b)] using the theoretical $\hat{\Delta}_{\text{MFT}}$ provides a correction prefactor, k_{mode}, that increases as $\delta\hat{\varphi} = \hat{\varphi} - \hat{\varphi}_{\text{d}}$ shrinks. (If $\hat{\Delta}_{\text{MFT}}$ is left as a fit parameter, its deviation from the theoretical prediction is $\lesssim 5\%$ consistently with the numerical uncertainty of the data.) Remarkably, perturbative corrections to MFT become increasingly pronounced upon approaching $\hat{\varphi}_{\text{d}}$. Two processes beyond the $d \to \infty$ MFT description, however, also then appear: (i) the cage size distribution displays a large-$\hat{\Delta}$ tail, and (ii) a substantial fraction of tracers escape the shell. As a result, within the range of system sizes and dimensions accessible in numerical simulations, the mode no longer converges to the MFT prediction for $\hat{\varphi} < 2.45$.

In order to disentangle these two different physical contributions and to resolve how the MFT description emerges as d increases, we consider the first-passage time of the tracer escaping from a center displacement $\sqrt{\hat{\Delta}_{\text{esc}}}$. For a fixed scaled density $\hat{\varphi} > \hat{\varphi}_{\text{d}}$, the onset of cage escapes is found to be exponentially delayed in time with increasing dimension for $d \geqslant 8$ [Fig. 4(d)]. More precisely, the cumulative probability of a tracer escaping, $P_{\text{esc}}(\hat{t})$, at fixed $\hat{\varphi}$ follows a scaling form

$$P_{\text{esc}}(\hat{t}; \delta\hat{\varphi}) \sim \hat{f}(e^{-C_{\text{esc}}d\delta\hat{\varphi}\hat{t}}; \delta\hat{\varphi}), \tag{6}$$

with master function $\hat{f}(x; \delta\hat{\varphi})$ and a prefactor $C_{\text{esc}}(\hat{\Delta}_{\text{esc}}) \approx 0.4$ that depends only weakly on the choice of cutoff for $\hat{\Delta}_{\text{esc}}/\hat{\Delta}_{\text{mode}} \sim O(1)$. In small dimensions, however, cage escapes deviate from this scaling form. Mean-field-like caging around $\hat{\varphi}_{\text{d}}$ is then so weak that higher-order corrections dominate.

We can now properly understand the logarithmic drift of the MSD that appears at intermediate times when $\hat{\varphi}_{\text{p}} > \hat{\varphi}_{\text{d}}$ as being due to imperfect caging. As dimension increases, the MFT caging prediction is recovered because the prefactor of the logarithm slowly vanishes. Geometrically, most cages are open for $\hat{\varphi}_{\text{d}} < \hat{\varphi} < \hat{\varphi}_{\text{p}}$, thus giving rise to void percolation, but escape paths out of open cages steadily shrink with increasing d, giving rise to more pronounced dynamical caging. This collapse form further suggests that near $\hat{\varphi}_{\text{d}}$ cage escapes are so prevalent that they dominate the dynamics in any finite d. Such *hopping* processes (exponentially suppressed in d by contrast to $1/d$ perturbations) have long been debated in glass physics [36–38], but this particular instantonic correction to the MFT of glasses was previously unknown. More than a mere correction, it is here found to be the primary reason why the sharp mean-field dynamical glass transition becomes a crossover in finite d.

Conclusion. Analyzing the interplay between glassiness and percolation in the RLG here establishes that the RLG dynamics is identical to that of hard-sphere glasses in $d \to \infty$ over finite timescales, and provides quantitative evidence of nontrivial finite-dimensional corrections to MFT. More specifically, we have found that the static cage size at high density and the typical dynamical cage size at all densities show a *perturbative*, $1/d$, correction to the MFT $d \to \infty$ result, and that *nonperturbative* dynamical cage escapes are suppressed exponentially with d around $\hat{\varphi}_{\text{d}}$. In

the RLG, these finite-dimensional corrections are dominant in physical dimensions, $d = 2, 3$. Our work therefore reveals in a precise and concrete way the important role played by activated processes in avoiding the dynamical glass transition.

Having identified these two types of corrections to MFT that go beyond the traditional instantonic picture [39] and facilitation [40], we should now be able to identify activated processes for more realistic models of glasses and obtain first-principle description of nonperturbative corrections to MFT for finite-dimensional disordered systems. Our results also suggest a putative first-principle pathway for relating local structure and dynamics in glass-forming liquids [41].

[1] J. Kertesz, J. Phys. Lett. **42**, 393 (1981).

[2] W. T. Elam, A. R. Kerstein, and J. J. Rehr, Phys. Rev. Lett. **52**, 1516 (1984).

[3] D. Stauffer and A. Aharony, *Introduction to Percolation Theory* (Taylor & Francis, London, 1994).

[4] D. Ben-Avraham and S. Havlin, *Diffusion and Reactions in Fractals and Disordered Systems* (Cambridge University Press, Cambridge, UK, 2000).

[5] F. Höfling, T. Franosch, and E. Frey, Phys. Rev. Lett. **96**, 165901 (2006).

[6] A. Dmitriev, M. Dyakonov, and R. Jullien, Phys. Rev. Lett. **89**, 266804 (2002).

[7] F. Höfling and T. Franosch, Rep. Prog. Phys. **76**, 046602 (2013).

[8] J. D. Treado, Z. Mei, L. Regan, and C. S. O'Hern, Phys. Rev. E **99**, 022416 (2019).

[9] W. Götze, E. Leutheusser, and S. Yip, Phys. Rev. A **23**, 2634 (1981).

[10] E. Leutheusser, Phys. Rev. A **29**, 2765 (1984).

[11] G. Szamel, Europhys. Lett. **65**, 498 (2004).

[12] Y. Jin and P. Charbonneau, Phys. Rev. E **91**, 042313 (2015).

[13] V. Krakoviack, Phys. Rev. E **75**, 031503 (2007).

[14] K. Kim, K. Miyazaki, and S. Saito, Europhys. Lett. **88**, 36002 (2009).

[15] J. Kurzidim, D. Coslovich, and G. Kahl, Phys. Rev. Lett. **103**, 138303 (2009).

[16] G. Szamel and E. Flenner, Europhys. Lett. **101**, 66005 (2013).

[17] B. Coluzzi, M. Mézard, G. Parisi, and P. Verrocchio, J. Chem. Phys. **111**, 9039 (1999).

[18] I. Biazzo, F. Caltagirone, G. Parisi, and F. Zamponi, Phys. Rev. Lett. **102**, 195701 (2009).

[19] H. Ikeda, K. Miyazaki, and A. Ikeda, J. Chem. Phys. **145**, 216101 (2016).

[20] G. Parisi, P. Urbani, and F. Zamponi, *Theory of Simple Glasses: Exact Solutions in Infinite Dimensions* (Cambridge University Press, Cambridge, UK, 2020), Chap. 4.

[21] G. Biroli, P. Charbonneau, and Y. Hu, Phys. Rev. E **99**, 022118 (2019).

[22] G. Parisi and F. Zamponi, Rev. Mod. Phys. **82**, 789 (2010).

[23] See Supplemental Material at http://link.aps.org/supplemental/10.1103/PhysRevE.103.L030104 for a detailed description of the notation, the mean-field theory derivation, the void percolation threshold computation, the optimal periodic box choice, and the numerical cavity reconstruction schemes.

[24] A. R. Kerstein, J. Phys. A **16**, 3071 (1983).

[25] M. E. J. Newman and R. M. Ziff, Phys. Rev. E **64**, 016706 (2001).

[26] S. Mertens and C. Moore, Phys. Rev. E **86**, 061109 (2012).

[27] J. H. Convay and N. J. A. Sloane, IEEE Trans. Inf. Theory **28**, 227 (1982).

[28] J.-D. Boissonnat and C. Delage, *European Symposium on Algorithms* (Springer, New York, 2005), pp. 367–378.

[29] A. V. Tomilov, Header-only single-class implementation of the quickhull algorithm for convex hulls finding in arbitrary dimension space (2016), based on [44,45].

[30] Z. Koza and J. Poła, J. Stat. Mech. Theory Exp. (2016) 103206.

[31] P. Charbonneau, Y. Jin, G. Parisi, and F. Zamponi, Proc. Natl. Acad. Sci. USA **111**, 15025 (2014).

[32] S. Sastry, D. S. Corti, P. G. Debenedetti, and F. H. Stillinger, Phys. Rev. E **56**, 5524 (1997).

[33] P. L. Leath, Phys. Rev. B **14**, 5046 (1976).

[34] F. Höfling, T. Munk, E. Frey, and T. Franosch, J. Chem. Phys. **128**, 164517 (2008).

[35] L. Berthier, P. Charbonneau, and J. Kundu, Phys. Rev. Lett. **125**, 108001 (2020).

[36] W. Gotze and L. Sjogren, J. Phys. C **21**, 3407 (1988).

[37] S. M. Bhattacharyya, B. Bagchi, and P. G. Wolynes, Phys. Rev. E **72**, 031509 (2005).

[38] S. Mirigian and K. S. Schweizer, J. Chem. Phys. **140**, 194507 (2014).

[39] M. Dzero, J. Schmalian, and P. G. Wolynes, Phys. Rev. B **72**, 100201(R) (2005).

[40] L. Berthier and G. Biroli, Rev. Mod. Phys. **83**, 587 (2011).

[41] C. P. Royall and S. R. Williams, Phys. Rep. **560**, 1 (2015).

[42] R. Pordes, D. Petravick, B. Kramer, D. Olson, M. Livny, A. Roy, P. Avery, K. Blackburn, T. Wenaus, F. Würthwein, I. Foster, R. Gardner, M. Wilde, A. Blatecky, J. McGee, and R. Quick, J. Phys.: Conf. Ser. **78**, 012057 (2007).

[43] I. Sfiligoi, D. C. Bradley, B. Holzman, P. Mhashilkar, S. Padhi, and F. Wurthwein, in *2009 WRI World Congress on Computer Science and Information Engineering* (IEEE, New York, 2009), Vol. 2, pp. 428–432.

[44] C. B. Barber, D. P. Dobkin, D. P. Dobkin, and H. Huhdanpaa, ACM Trans. Math. Softw. **22**, 469 (1996).

[45] K. Mehlhorn, S. Näher, M. Seel, R. Seidel, T. Schilz, S. Schirra, and C. Uhrig, Comput. Geom. **12**, 85 (1999).

[46] https://doi.org/10.7924/r4qz29054